Electronic Supplementary Material (ESI) for Journal of Materials Chemistry A

The First Single-Sized (~1 nm) and Periodically Ordered Array of In_2Te_3 Semiconductor Quantum Dots Self-Assembled in Solution

Ruibo Zhang,[†] Thomas J. Emge,[†] Chong Zheng,[‡] and Jing Li*,[†]

[†]Department of Chemistry and Chemical Biology, Rutgers, The State University of New Jersey, Piscataway, NJ 08854
[‡]Department of Chemistry and Biochemistry, Northern Illinois University, DeKalb, IL 60115

Supporting Information

Experimental Details

Materials: Indium(III) chloride (anhydrous, 98%) and triethylenetetramine (tech. 60%) were purchased from Alfa Aesar. Na_2TeO_3 was purchased from Kanto Chemical. All chemicals were used as-received without further treatment.

Synthesis of $[In_8Te_{12}(trien)_4]$ crystals: A mixture of $InCl_3$ (0.110g, 0.5 mmol) and Na_2TeO_3 (0.111g, 0.5 mmol) was placed in a 23 mL Teflon liner; 4 mL of triethylenetetramine (*trien*) was then added. The mixture was stirred for 20 min and subsequently sealed in a Parr autoclave. The reaction took place in a programmable oven at 150 °C for 3 days. The autoclave was then cooled down to the room temperature at a rate of 0.1 °C min^{-1}. After the filtration, the product (yellow sheet-like crystals) was washed several times with distilled water and absolute ethanol, and dried under vacuum for 1 h. Yield: 61%.

Dispersion of $[In_8Te_{12}(trien)_4]$ nanoparticles: A small amount (0.01-0.05 mmol) of the title compound was added to 40 mL of absolute ethanol; 10 mL of PEG (polyethylene glycol, M=10000) was then added dropwise under stirring. After stirring for 1h, the resultant mixture was sonicated at 60-70 °C for 2h (3 s on, 1 s off, amplitude 30%) by using an ultrasound processor (Sonics and Materials, VC750, 20 KHz) with a microtip probe. The so-obtained suspension was left to cool down to the room temperature. The powder product was collected by centrifugation, followed by washing in deionized water and drying under vacuum at room temperature.

Diffuse reflectance measurements: Optical diffuse reflectance spectra were collected on a Shimadzu UV-3101PC double-beam, double-monochromator spectrophotometer in the wavelength range of 250 to 2000 nm at room temperature. $BaSO_4$ powder was used as a 100% standard reflectance. A previously described procedure was used to convert the data through the Kubelka-Munk function [19]. The scattering coefficient (S) was treated as a constant because the average particle size of the tested sample was significantly larger than 5 μm.

Powder X-ray diffraction: Powder X-ray diffraction (PXRD) patterns were measured on a Rigaku D/M-2200T diffraction system (Ultima+). Measurements were performed in a 2θ range of 3-50° (Cu Kα radiation, λ = 1.5406 Å). The data were collected at room temperature with a step size of 0.02° (2θ) and a scan rate of 3° min^{-1}. The operating power was 40 kV/40 mA.

Thermogravimetric (TG) analysis: TG analysis of a polycrystalline sample of **1** was performed on a TA Instruments Q50 TG analyzer. The powder sample was loaded into a ceramic pan and heated with a ramp rate of 10 °C min^{-1} from room temperature to 600 °C under nitrogen (flow and purge rate at 40mL min^{-1} and 60 mL min^{-1}, respectively).

Single crystal X-ray crystallography: Single crystal X-ray diffraction data were collected at 100(2)K on a Bruker-AXS Smart APEX II CCD diffractometer with graphite-monochromated Mo Kα radiation (λ = 0.71073 Å). The structure was solved by direct methods and refined by full-matrix least-squares on F^2 using the SHELX-97 program package. Crystal data: $C_{24}H_{72}In_8N_{16}Te_{12}$, Fw = 3034.74, Monoclinic, *C*2/*c*, *a* = 28.720(3), *b* = 15.8481(11), *c* = 14.2792(10) Å, *V* = 6394.1(8) $Å^3$, *Z* = 4, D_c = 3.152 gcm^{-3}, *R*1 = 0.0514, *wR*2 = 0.1366 ($I > 2\sigma(I)$), GoF = 1.008. CCDC 833180 contains the supplementary crystallographic data for this paper. These data can be obtained free of charge from The Cambridge Crystallographic Data Centre via www.ccdc.cam.ac.uk/data_request/cif.

Electron microscopy measurements: Samples for TEM analysis were prepared by deposition of a drop of particle in chloroform solution onto a carbon-coated copper grid. Conventional Transmission Electron Microscopy was performed on a JEM-100CXII electron microscope (JEOL) at 80 kV.

First-principles calculations: Calculations of band structure (BS) and density of states (DOS) were carried out for [In_8Te_{12}(*trien*)$_4$] and α-In_2Te_3 using a plane wave code of CASTEP.[1] The total energy was calculated by density functional theory (DFT) within the framework of nonlocal generalized gradient gradient-corrected approximations (i.e., Perdew-Burke-Ernzerhof (PBE) functional). The valence electronic configurations used for In, Te, C, N and H are $4d^{10}5s^25p^1$, $5s^25p^4$, $2s^22p^2$, $2s^22p^3$ and $1s^1$, respectively. The interactions between the ionic cores and electrons are described by the ultrasoft pseudopotential. The number of plane waves included in the basis is determined by a cutoff energy (310 eV for [In_8Te_{12}(*trien*)$_4$], 290 eV for α-In_2Te_3) and the numerical integration of the Brillouin zone is performed using a Monkhorst-Pack grid (1 × 1 × 1 for [In_8Te_{12}(*trien*)$_4$], 2 × 2 × 2 for α-In_2Te_3).

Figures and Tables

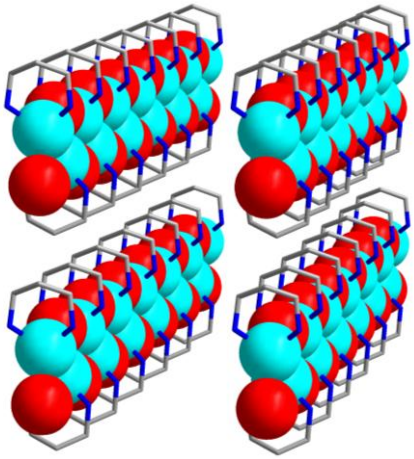

(a)

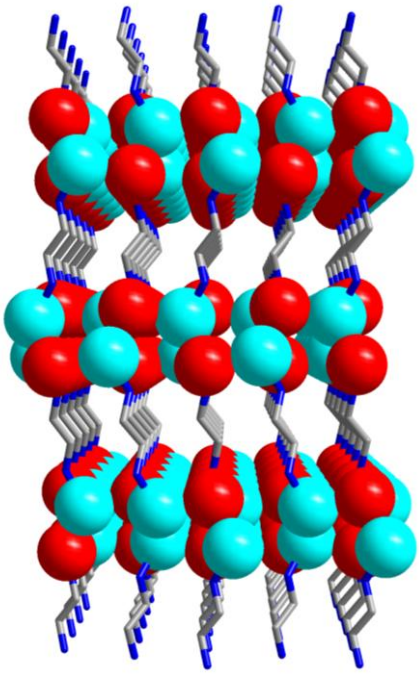

(b)

Figure S1. Views of single-sized ZnSe modules in the hybrid semiconductors based on II-VI binary phases: (**a)** single-atomic 1D chains and, (**b**) single-atomic 2D layers. These modules are at sub-nanometer scale and are interconnected or separated by organic molecules via coordinative bonds. Turquoise: Zn; red: Se; blue: N, gray, C.

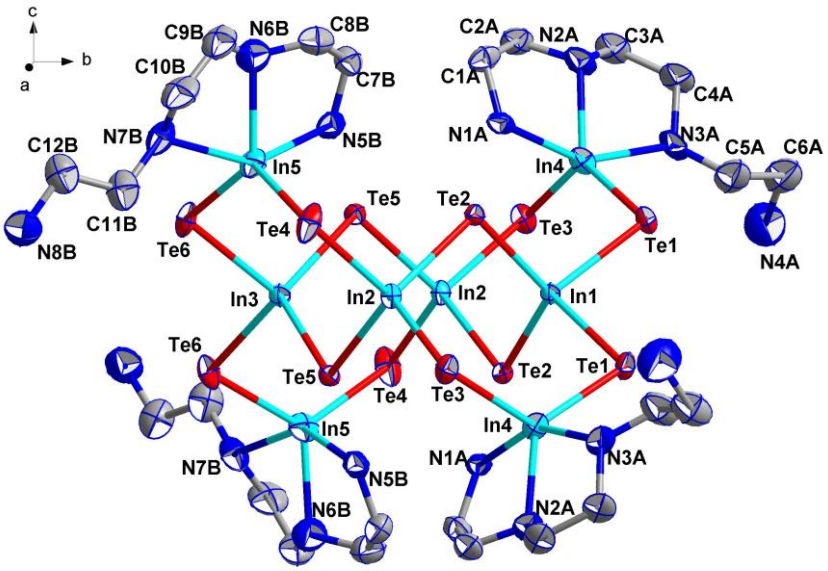

Figure S2. ORTEP drawing of $[In_8Te_{12}(trien)_4]$ showing the atom-labeling system in 50% thermal ellipsoids . Hydrogen atoms and the disordered C, N atoms are omitted for clarity.

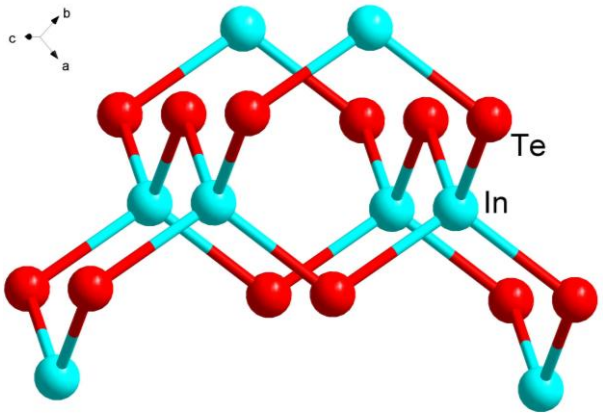

(a)

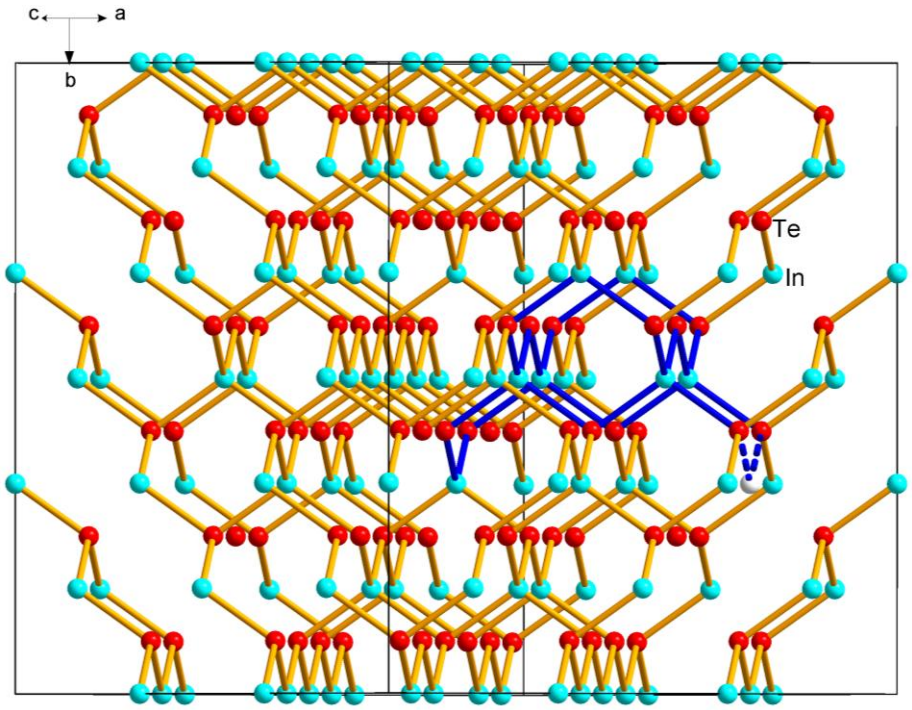

(b)

Figure S3. Views showing the structural similarity between (**a**) the $\{In_8Te_{12}\}$ cluster in the hybrid structure $[In_8Te_{12}(\textit{trien})_4]$ and, (**b**) the $\{In_8Te_{11}\}$ cluster in α-In_2Te_3.

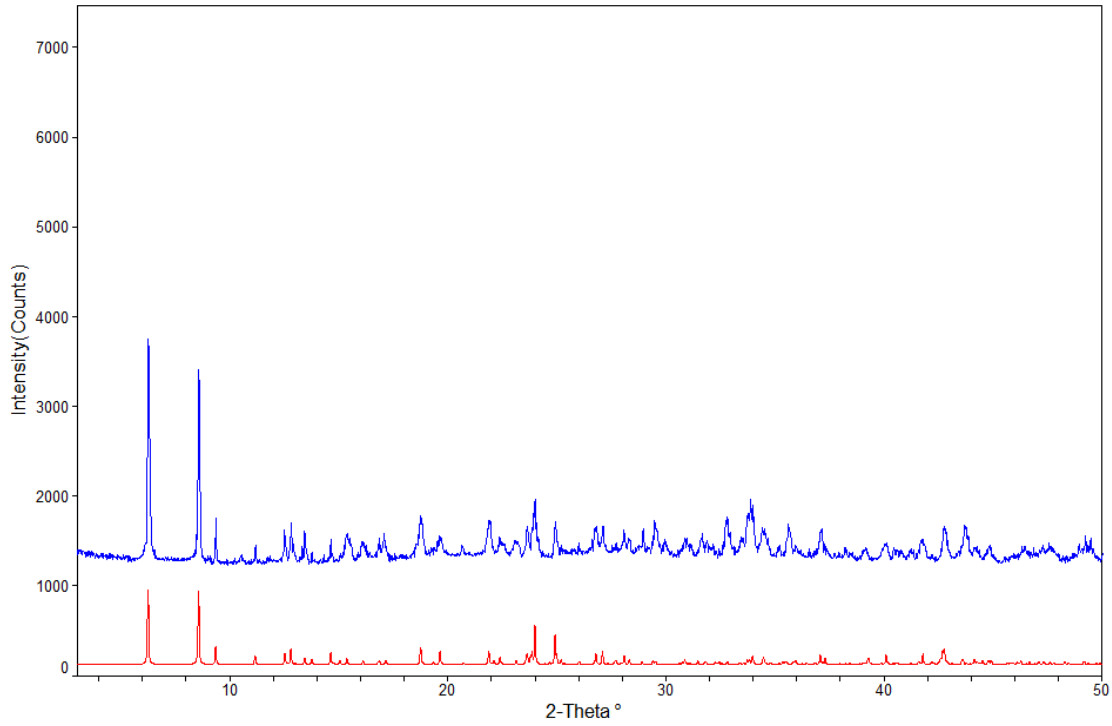

Figure S4. Powder X-ray diffraction patterns: as-made $[In_8Te_{12}(trien)_4]$ powder (blue); simulated from single-crystal X-ray data (red).

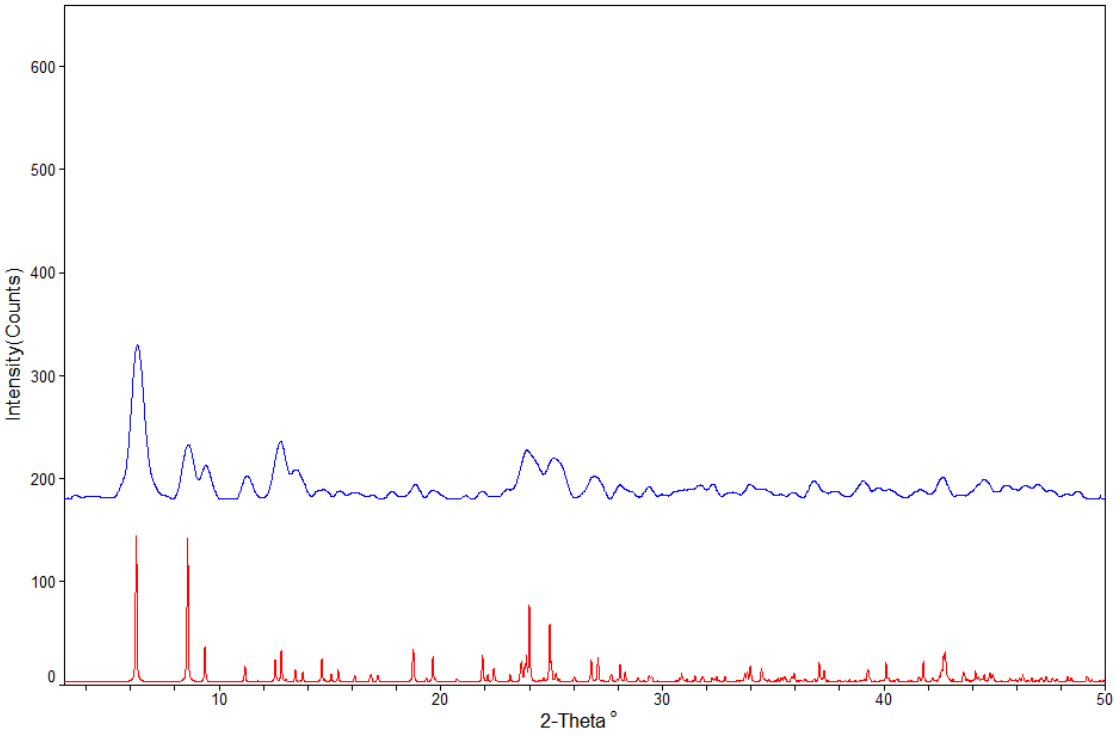

Figure S5. Powder X-ray diffraction patterns: dispersed $[In_8Te_{12}(trien)_4]$ nanoparticles (blue); simulated from single-crystal X-ray data (red).

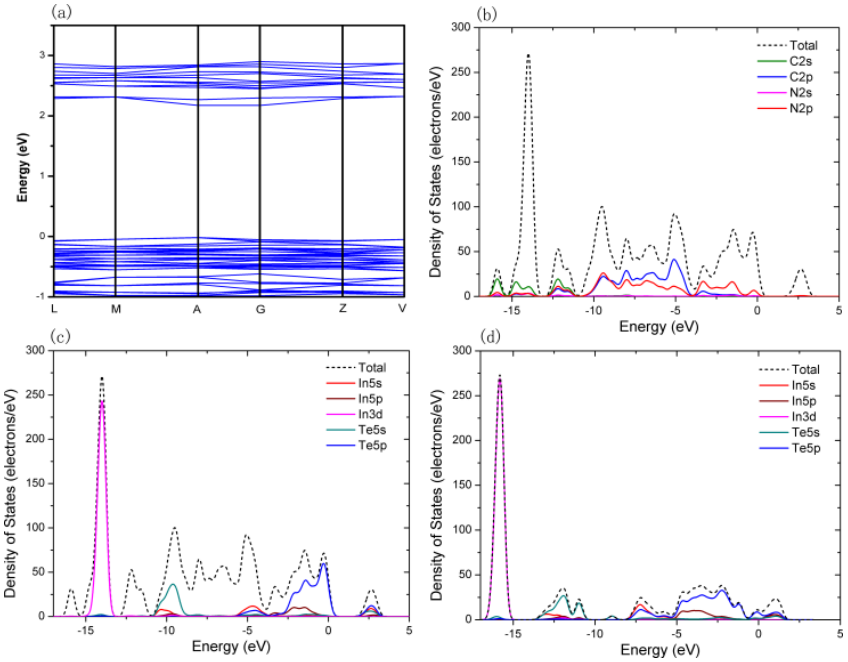

Figure S6. (a) Band structure of [In_8Te_{12}(*trien*)$_4$]. (b) and (c) Total and partial DOS of [In_8Te_{12}(*trien*)$_4$]. (d) Total and partial DOS of α-In_2Te_3. A larger version of this figure on is provided in the Supporting Information.

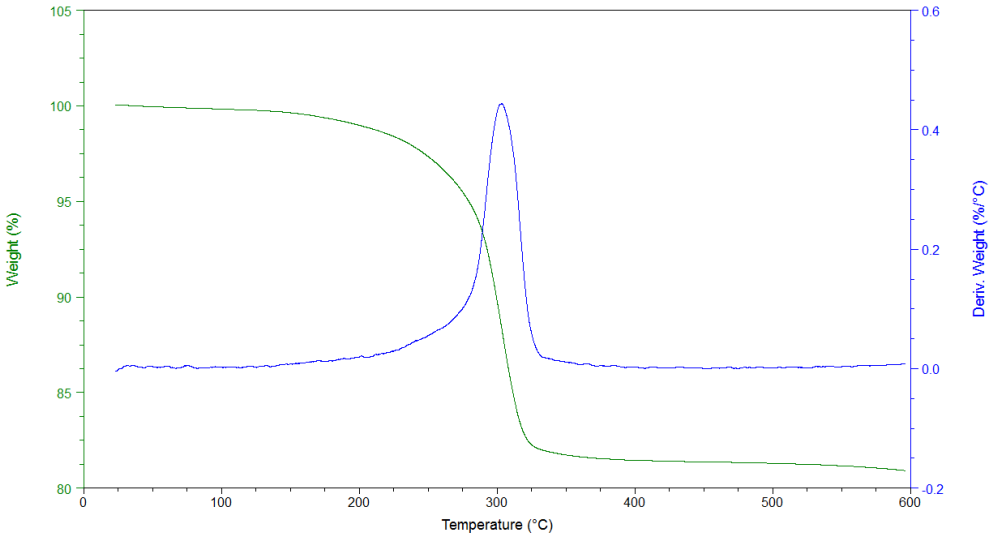

Figure S7. Thermogravimetric (TG) profile of [In_8Te_{12}(*trien*)$_4$]. The onset of sample decomposition is at ~180 °C, followed by a weight loss of 18.56% between 180 and 330 °C (calcd. 19.24%).

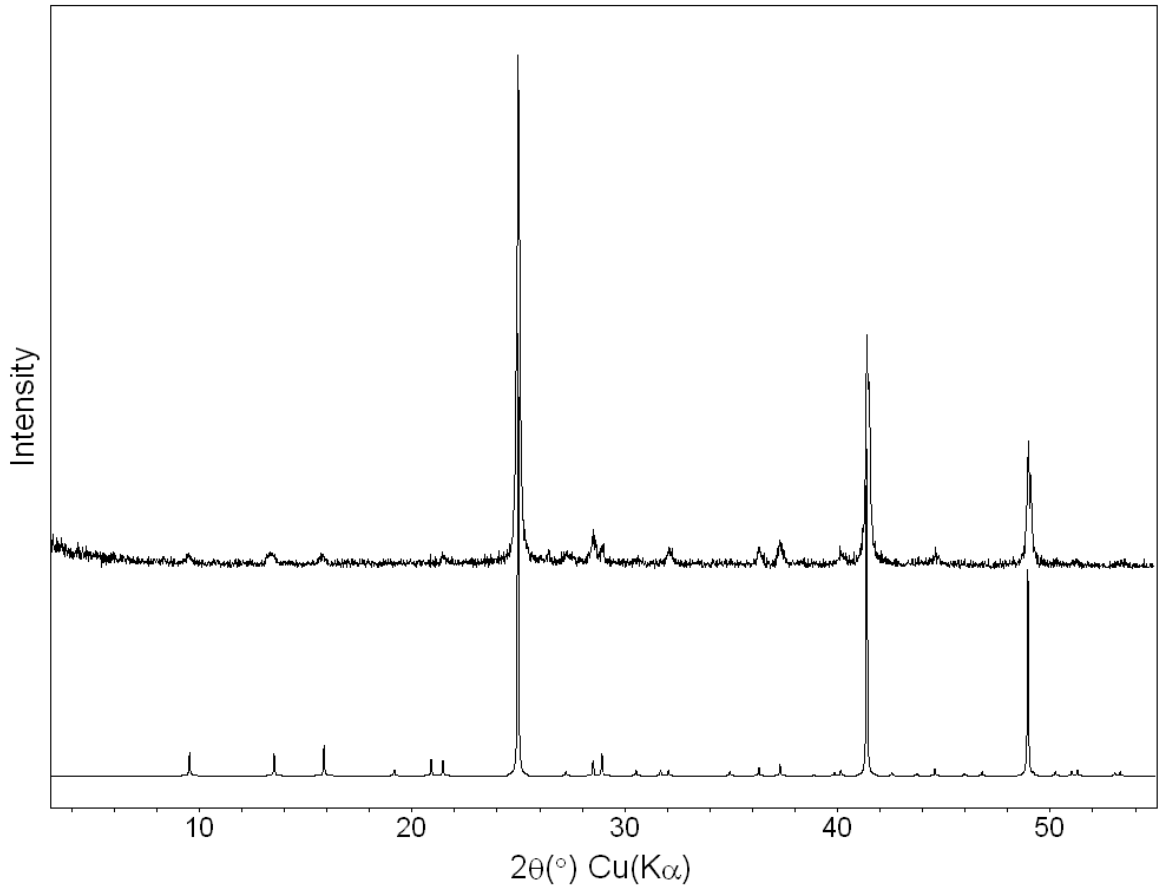

Figure S8. Power X-ray diffraction patterns. Top: In_2Te_3 powder (purchased from Sigma-Aldrich, 99.999% trace metals basis); Bottom: Simulated from the ICSD data of α-In_2Te_3 (S.G., $F\bar{4}3m$).

Table S1. Selected Bond Lengths (Å) and Angles (°) for $[In_8Te_{12}(trien)_4]^a$

In(1)-Te(2)	2.7498(7)	In(3)-Te(6)#1	2.7900(8)	In(4)-N(3B)	2.531(12)
In(1)-Te(2)#1	2.7498(7)	In(3)-Te(6)	2.7900(8)	In(4)-Te(3)#1	2.7284(9)
In(1)-Te(1)	2.7926(8)	Te(1)-In(4)	2.7059(9)	In(5)-N(5A)	2.308(8)
In(1)-Te(1)#1	2.7926(8)	Te(3)-In(4)#1	2.7285(9)	In(5)-N(7B)	2.341(12)
In(2)-Te(5)	2.7508(8)	Te(4)-In(5)#1	2.7112(11)	In(5)-N(6B)	2.311(14)
In(2)-Te(2)	2.7597(8)	Te(6)-In(5)	2.7242(10)	In(5)-N(6A)	2.385(14)
In(2)-Te(4)	2.7749(9)	In(4)-N(2A)	2.178(12)	In(5)-N(7A)	2.454(12)
In(2)-Te(3)	2.8027(8)	In(4)-N(1A)	2.317(8)	In(5)-Te(4)#1	2.7113(11)
In(3)-Te(5)#1	2.7715(7)	In(4)-N(2B)	2.432(14)		
In(3)-Te(5)	2.7715(7)	In(4)-N(3A)	2.397(11)		
Te(2)-In(1)-Te(2)#1	121.62(4)	In(2)-Te(5)-In(3)	103.24(2)	Te(1)-In(4)-Te(3)#1	124.97(3)
Te(2)-In(1)-Te(1)	106.777(18)	In(5)-Te(6)-In(3)	99.03(3)	N(5A)-In(5)-N(7B)	144.7(5)
Te(2)#1-In(1)-Te(1)	110.959(18)	N(2A)-In(4)-N(1A)	75.7(4)	N(5A)-In(5)-N(6B)	74.0(4)
Te(2)-In(1)-Te(1)#1	110.961(18)	N(2A)-In(4)-N(2B)	6.4(5)	N(7B)-In(5)-N(6B)	73.2(5)
Te(2)#1-In(1)-Te(1)#1	106.778(18)	N(1A)-In(4)-N(2B)	70.8(3)	N(5A)-In(5)-N(6A)	72.6(4)
Te(1)-In(1)-Te(1)#1	96.99(3)	N(2A)-In(4)-N(3A)	76.7(4)	N(7B)-In(5)-N(6A)	80.7(6)
Te(5)-In(2)-Te(2)	115.73(3)	N(1A)-In(4)-N(3A)	151.6(4)	N(6B)-In(5)-N(6A)	19.6(6)
Te(5)-In(2)-Te(4)	112.24(3)	N(2B)-In(4)-N(3A)	82.1(5)	N(5A)-In(5)-N(7A)	136.8(5)
Te(2)-In(2)-Te(4)	106.52(3)	N(2A)-In(4)-N(3B)	64.7(5)	N(7B)-In(5)-N(7A)	10.7(4)
Te(5)-In(2)-Te(3)	107.66(3)	N(1A)-In(4)-N(3B)	140.0(5)	N(6B)-In(5)-N(7A)	63.6(6)
Te(2)-In(2)-Te(3)	112.39(3)	N(2B)-In(4)-N(3B)	70.1(4)	N(6A)-In(5)-N(7A)	70.1(5)
Te(4)-In(2)-Te(3)	101.43(3)	N(3A)-In(4)-N(3B)	12.0(4)	N(5A)-In(5)-Te(4)#1	107.5(2)
Te(5)#1-In(3)-Te(5)	121.79(4)	N(2A)-In(4)-Te(1)	128.0(5)	N(7B)-In(5)-Te(4)#1	96.7(5)
Te(5)#1-In(3)-Te(6)#1	104.69(2)	N(1A)-In(4)-Te(1)	97.94(18)	N(6B)-In(5)-Te(4)#1	112.0(4)
Te(5)-In(3)-Te(6)#1	111.694(19)	N(2B)-In(4)-Te(1)	131.8(6)	N(6A)-In(5)-Te(4)#1	93.5(4)
Te(5)#1-In(3)-Te(6)	111.697(19)	N(3A)-In(4)-Te(1)	93.7(4)	N(7A)-In(5)-Te(4)#1	96.0(5)

Te(5)-In(3)-Te(6)	104.69(2)	N(3B)-In(4)-Te(1)	101.8(5)	N(5A)-In(5)-Te(6)	95.8(2)
Te(6)#1-In(3)-Te(6)	100.32(4)	N(2A)-In(4)-Te(3)#1	106.3(5)	N(7B)-In(5)-Te(6)	90.6(4)
In(4)-Te(1)-In(1)	99.80(3)	N(1A)-In(4)-Te(3)#1	103.54(19)	N(6B)-In(5)-Te(6)	122.0(4)
In(1)-Te(2)-In(2)	102.82(2)	N(2B)-In(4)-Te(3)#1	103.2(5)	N(6A)-In(5)-Te(6)	141.1(4)
In(4)#1-Te(3)-In(2)	98.17(3)	N(3A)-In(4)-Te(3)#1	90.5(4)	N(7A)-In(5)-Te(6)	99.6(4)
In(5)#1-Te(4)-In(2)	97.85(3)	N(3B)-In(4)-Te(3)#1	93.0(6)	Te(4)#1-In(5)-Te(6)	125.24(4)

[a] Symmetry codes: #1 -x, y, -z-1/2.

Table S2. Selected Bond Lengths (Å) and Angles (°) for α-In_2Te_3

In(1)-Te(2)	2.6688	In2-Te(3)	2.6699	In2-Te(5)	2.6688
In(1)-Te(5)	2.6677	In2-Te(4)	2.6677		
Te(2)-In(1)-Te(5)	109.49	Te(5)-In(2)-Te(3)	109.42	Te(5)-In(2)-Te(4)	109.49
Te(3)-In(2)-Te(4)	109.5				

Table S3. Experimental and Theoretically calculated Band Gap and Blue Shift Values

Compound	Band Gap (eV)		Blue Shift (eV)	
	calc.	expt.	calc.	expt.
[In_8Te_{12}(*trien*)$_4$]	2.11	2.7	2.05	2.1
α-In_2Te_3	0.06	0.6		

References

[1] S. J. Clark, M. D. Segall, C. J. Pickard, P. J. Hasnip, M. J. Probert, K. Refson, M. C. Payne, *Zeitschrift Fur Kristallographie* **2005**, *220*, 567-570.